A peer-reviewed version of this preprint was published in PeerJ on 6 December 2018.

View the peer-reviewed version (peerj.com/articles/6072), which is the preferred citable publication unless you specifically need to cite this preprint.

Jin W, Liang X, Brooks A, Futrega K, Liu X, Doran MR, Simpson MJ, Roberts MS, Wang H. 2018. Modelling of the SDF-1/CXCR4 regulated *in vivo* homing of therapeutic mesenchymal stem/stromal cells in mice. PeerJ 6:e6072 https://doi.org/10.7717/peerj.6072

Modelling of the SDF-1/CXCR4 regulated *in vivo* homing of therapeutic mesenchymal stem/stromal cells in mice

Wang Jin [1], **Xiaowen Liang** [2], **Anastasia Brooks** [2], **Kathryn Futrega** [3], **Xin Liu** [2], **Michael R. Doran** [3,4,5], **Matthew J. Simpson** [1], **Michael S. Roberts** [Corresp., 2,6], **Haolu Wang** [Corresp. 2]

[1] School of Mathematical Sciences, Queensland University of Technology, Brisbane, Australia

[2] Therapeutics Research Centre, The University of Queensland Diamantina Institute, University of Queensland, Translational Research Institute, Brisbane, Australia

[3] Institute of Health and Biomedical Innovation, Queensland University of Technology, Translational Research Institute, Brisbane, Australia

[4] Mater Research Institute, University of Queensland, Translational Research Institute, Brisbane, Australia

[5] Australian National Centre for the Public Awareness of Science, Australian National University, Canberra, Australia

[6] School of Pharmacy and Medical Science, University of South Australia, Adelaide, Australia

Corresponding Authors: Michael S. Roberts, Haolu Wang
Email address: sallee.goh@mater.uq.edu.au, h.wang21@uq.edu.au

Background. Mesenchymal stem/stromal cells (MSCs) are a promising tool for cell-based therapies in the treatment of tissue injury. The stromal cell-derived factor-1 (SDF-1)/CXC chemokine receptor 4 (CXCR4) axis plays a significant role in directing MSC homing to sites of injury. However *in vivo* MSC distribution following intravenous transplantation remains poorly understood, potentially hampering the precise prediction and evaluation of therapeutic efficacy.

Methods. A murine model of partial ischemia/reperfusion (I/R) is used to induce liver injury, increase the hepatic levels of SDF-1, and study *in vivo* MSC distribution. Hypoxia-preconditioning increases the expression of CXCR4 in human bone marrow-derived MSCs. Quantitative assays for human DNA allow us to examine the *in vivo* kinetics of intravenously infused human MSCs in mouse blood and liver. A mathematical model-based system is developed to characterize *in vivo* homing of human MSCs in mouse models with SDF-1 levels in liver and CXCR4 expression on the transfused MSCs. The model is calibrated to experimental data to provide novel estimates of relevant parameter values.

Results. Images of immunohistochemistry for SDF-1 in the mouse liver with I/R injury show a significantly higher SDF-1level in the I/R injured liver than that in the control. Correspondingly, the ELISA results illustrate a higher MSC dose in the I/R injured liver than the normal liver. CXCR4 is overexpressed in hypoxia-preconditioned MSCs. An increased number of hypoxia-preconditioned MSCs in the I/R injured liver is observed from the ELISA results. The model simulations align with the experimental data of control and hypoxia-preconditioned human MSC distribution in normal and injured mouse livers, and accurately predict the experimental outcomes with different MSC doses.

Discussion. The modelling results suggest that SDF-1 in organs is an effective *in vivo* attractant for MSCs through the SDF-1/CXCR4 axis and reveals the significance of the SDF-1/CXCR4 chemotaxis on *in vivo* homing of MSCs, especially under hypoxic preconditioning. The impact of the liver and MSC conditions on passive homing is small. This *in vivo* modelling approach allows qualitative characterization and prediction of the MSC homing to normal and injured organs on the basis of clinically accessible variables, such as the MSC dose and SDF-1 concentration in blood. This model could also be adapted to abnormal conditions and/or other types of circulating cells to predict *in vivo* homing patterns.

Modelling of the SDF-1/CXCR4 Regulated *In vivo* Homing of Therapeutic Mesenchymal Stem/stromal Cells In Mice

Wang Jin[a], Xiaowen Liang[b], Anastasia Brooks[b], Kathryn Futrega[c], Xin Liu[b], Michael R. Doran[c,d,e], Matthew J. Simpson[a], Michael S. Roberts[b,f], Haolu Wang[b]

[a] School of Mathematical Sciences, Queensland University of Technology, Brisbane, Australia

[b]Therapeutics Research Centre, The University of Queensland Diamantina Institute, The University of Queensland, Translational Research Institute, Brisbane, Australia

[c]Institute of Health and Biomedical Innovation, Queensland University of Technology, Translational Research Institute, Brisbane, Australia

[d]Mater Research Institute, The University of Queensland, Translational Research Institute, Brisbane, Australia

[e]Australian National Centre for the Public Awareness of Science, Australian National University, Canberra, Australia

[f]School of Pharmacy and Medical Science, University of South Australia, Adelaide, Australia

Correspondence: Michael S. Roberts, Ph.D., The University of Queensland Diamantina Institute, The University of Queensland, Translational Research Institute, QLD 4103, Australia. Telephone: 61-07-3443-8033; Email: m.roberts@uq.edu.au and Haolu Wang, MBBS., Ph.D., The University of Queensland Diamantina Institute, The University of Queensland, Translational Research Institute, QLD 4103, Australia. Telephone: 61-07-3443-7488; Email: h.wang21@uq.edu.au

ABSTRACT

Background. Mesenchymal stem/stromal cells (MSCs) are a promising tool for cell-based therapies in the treatment of tissue injury. The stromal cell-derived factor-1 (SDF-1)/CXC chemokine receptor 4 (CXCR4) axis plays a significant role in directing MSC homing to sites of injury. However *in vivo* MSC distribution following intravenous transplantation remains poorly understood, potentially hampering the precise prediction and evaluation of therapeutic efficacy.

Methods. A murine model of partial ischemia/reperfusion (I/R) is used to induce liver injury, increase the hepatic levels of SDF-1, and study *in vivo* MSC distribution. Hypoxia-preconditioning increases the expression of CXCR4 in human bone marrow-derived MSCs. Quantitative assays for human DNA allow us to examine the *in vivo* kinetics of intravenously infused human MSCs in mouse blood and liver. A mathematical model-based system is developed to characterize *in vivo* homing of human MSCs in mouse models with SDF-1 levels in liver and CXCR4 expression on the transfused MSCs. The model is calibrated to experimental data to provide novel estimates of relevant parameter values.

Results. Images of immunohistochemistry for SDF-1 in the mouse liver with I/R injury show a significantly higher SDF-1level in the I/R injured liver than that in the control. Correspondingly, the ELISA results illustrate a higher MSC dose in the I/R injured liver than the normal liver. CXCR4 is overexpressed in hypoxia-preconditioned MSCs. An increased number of hypoxia-preconditioned MSCs in the I/R injured liver is observed from the ELISA results. The model simulations align with the experimental data of control and hypoxia-preconditioned human MSC distribution in normal and injured mouse livers, and accurately predict the experimental outcomes with different MSC doses.

Discussion. The modelling results suggest that SDF-1 in organs is an effective *in vivo* attractant for MSCs through the SDF-1/CXCR4 axis and reveals the significance of the SDF-1/CXCR4 chemotaxis on *in vivo* homing of MSCs, especially under hypoxic preconditioning. The impact of the liver and MSC conditions on passive homing is small. This *in vivo* modelling approach allows qualitative characterization and prediction of the MSC homing to normal and injured organs on the basis of clinically accessible variables, such as the MSC dose and SDF-1 concentration in blood. This model could also be adapted to abnormal conditions and/or other types of circulating cells to predict *in vivo* homing patterns.

1. INTRODUCTION

Mesenchymal stem/stromal cells (MSCs) are excellent candidates for use in tissue repair and regeneration (Jiang et al., 2018; Niclis et al., 2017; Squillaro et al., 2016; Zhang et al., 2017). Human MSCs can be harvested from a range of tissues (bone marrow and adipose are common sources) with few ethical issues; and MSC-based therapies have few adverse events (Parekkadan et al., 2010; Rohart et al., 2016; Zhang et al., 2017). Similar to the use of pharmacokinetics for drug development, the aim of elucidating *in vivo* kinetics of MSCs is to predict and enhance their therapeutic potential. Hence understanding *in vivo* kinetics of MSCs becomes a critical step in the development of any new therapeutic agent to establish the optimal dosing regimens and targeting strategies (Jin et al., 2016; Zhao et al., 2011).

One important mechanism that is often overlooked, but essential for MSC therapy is the homing of MSCs. There are several mediators and receptors involved in the homing of MSCs to sites of injury. A number of studies indicate that the stromal cell-derived factor-1 (SDF-1, also known as CXCL12) is upregulated at sites of injury and serves as a potent chemoattractant to recruit circulating or residing MSCs expressing its cognate receptor CXC chemokine receptor 4 (CXCR4) (**Fig. 1A**) (Dar et al., 2005; Ji et al., 2004). The SDF-1/CXCR4 axis promotes stem cell mobilization to injured organs such as brain (Ji et al., 2004), bone (Kitaori et al., 2009), skin (Hu et al., 2013), kidneys (Liu et al., 2012), heart (Abbott et al., 2004) and liver tissues (Kucia et al., 2004). Treating MSCs with hypoxia-preconditioning in culture induces high surface expression of CXCR4 that enhances homing ability (Ji et al., 2004).

In addition to experimental studies, cell kinetics have also been widely studied using various mathematical modelling frameworks to help understand both *in vitro* and *in vivo* mechanisms (Chung et al., 2008; Jin et al., 2016; Werner et al., 2015), and design clinical treatment protocols (Enderling et al., 2009; Werner et al., 2016; Wodarz et al., 2014). In general, there are two types of mathematical models used to study such biological systems: (i) Continuum models that measure population-level properties, such as the concentration or density of populations of cells, without dealing specifically with individual-level properties (Enderling et al., 2009; Jin et al., 2016; Werner et al., 2015; Werner et al., 2016; Wodarz et al., 2014); and (ii) Discrete models that directly simulate individual cells (Holzhütter et al., 2012; Jin et al., 2017). Sometimes, a multi-scale model can be established that predicts both individual- and population-level properties, and this is achieved by taking the continuum limit description of some particular discrete, individual-based model (Jin et al., 2016; Jin et al., 2018). The first model for the *in vivo* kinetics of MSCs is a population-level model, published in 2016 (Wang et al., 2016). This physiologically-based pharmacokinetic model can characterize and predict the organ distribution of administered MSCs. However, the model only considers active homing mechanisms via blood flow and neglects effects of tissue injury on MSC distribution (Wang et al., 2016; Zhu et al., 1996). As a result, the model underestimates the MSC doses in injured organs.

In this work we develop a mathematical model-based system to characterize the *in vivo* homing of administered human bone marrow-derived MSCs with SDF-1 levels in liver and CXCR4 expression on the transfused MSCs. This continuum model presented here is novel since it includes both passive and active homing mechanisms. The model shows good agreement with experimental data, and provides insights into passive and active homing mechanisms. The

calibrated model also accurately predicts outcomes with different MSC doses. This *in vivo* modelling approach enables qualitative characterization and prediction of the MSC homing to normal and injured organs.

2. MATERIALS AND METHODS

2.1 Hepatic ischemia-reperfusion (I/R) injury model.

All animal procedures are approved by the Animal Ethics Committee of the University of Queensland (MED/493/15/NHMRC) and are carried out in accordance with Australian Code for the Care and Use of Animals for Scientific Purposes 8th edition. Healthy mice (Male 20-week-old BALB/c nude) are anaesthetized initially by an intraperitoneally injection of ketamine hydrochloride (80 mg/kg) and xylazine (10 mg/kg). Body temperature is controlled by placing mice on a heating pad set to 37°C. Hepatic I/R injury is induced by clamping the portal vein and hepatic artery supplying the median and left lobes using a microvascular clamp. After 45 min of partial ischemia, the clamp is removed to allow reperfusion in the liver.

2.2 Hypoxia-precondition of human MSCs

Bone marrow aspirates are collected from fully informed healthy human volunteer donors who provided written consent. Ethical approval is granted through the Mater Health Services Human Research Ethics Committee and ratified by the Queensland University of Technology Human Ethics Committee (number: 1000000938). Human MSCs are isolated from bone marrow aspirates, cultured and characterized as we previously described (Parekkadan et al., 2010;

Squillaro et al., 2016). All cells are cultured in monolayer using expansion media formulated from low glucose DMEM (ThermoFischer) supplemented with 10% fetal bovine serum (FBS, ThermoFisher) and 10 ng/mL FGF-1 (Peprotech). All experiments involving MSCs are performed at passage 4-8, tested negative for mycoplasma contamination, and <80% confluence. MSCs are cultured in a hypoxia chamber incubator (catalog No. 27310; StemCell Technologies, Vancouver, BC, Canada) at 37 ^{o}C in 3% O_2, 5% CO_2 and 92% N_2 for 24 h, and these MSCs are named as hypoxia-preconditioned MSCs. MSCs cultured for 24 h in 95% air and 5% CO_2 are used as a control.

2.3 In vivo transplantation of MSCs

Male 20-week-old BALB/c nude mice are purchased from the Animal Resource Centre (Perth, Western Australia). 150 µl of a suspension of 5×10^5 or 1.5×10^6 MSCs is injected with a 27-gauge needle through the tail vein of the control mice or mice with hepatic I/R injury at the time of reperfusion. Prior to injection, the MSCs are maintained at 4°C, and the cells are gently resuspended with a pipette to ensure no aggregation before injection. Animals (n = 3) are sacrificed at designated times (30 min, 4, 15, 24, and 48 h post-injection). Blood is obtained by cardiac puncture. The normal liver and the liver with I/R injury are removed for analysis.

2.4 Droplet digital PCR assays for Alu sequences

Genomic DNA (gDNA) of the blood and liver are isolated using DNA Mini Kit (Qiagen, USA). Droplet digital PCR (ddPCR) is performed in reaction consisting of gDNA, primer sets (Alu

147 forward: GCCTGTAATCCCAGCACTTT; Alu reverse: CACTACGCCCGGCTAATTT) (Zhao
148 et al., 2011), H_2O and ddPCR EvaGreen Supermix (BioRad, USA). ddPCR is performed
149 according to manufacturer's manual. Briefly, 20μL of ddPCR reaction mix is separated into
150 droplets with QX200 Droplet Generator (BioRad, USA). The droplets are transferred into a 96-
151 well PCR plate, sealed and incubated at following cycling conditions: one cycle of 95ºC for 5
152 minutes, 45 cycles of 95ºC for 30 seconds, 55ºC for 1 minute and one cycle of 4ºC for 5 minutes,
153 90ºC for 5 minutes and an infinite hold of 12ºC. After thermal cycling, the PCR plate is
154 transferred in QX200 Droplet Reader (read) and read in FAM channel using QuantaSoft version
155 1.7.
156
157 *2.5 Quantitative ELISA analysis*
158
159 Liver samples are weighed and immediately placed in 10 volumes (wt/vol) of a protease inhibitor
160 cocktail containing 10 nmol/l EDTA, 2 mmol/l PMSF, 0.1 mg/ml soybean trypsin inhibitor, 1.0
161 mg/ml bovine serum albumin, and 0.002% sodium azide in isotonic PBS, pH 7.0. Tissues are
162 disrupted with a tissue homogenizer, and lysates are incubated at 4°C for 2 h. Samples are
163 clarified by two rounds of centrifugation at 12,500 g for 10 min at 4°C. SDF-1 concentrations in
164 blood and liver are assessed by enzyme-linked immunosorbent assay (CUSABIO, TX, USA).
165 CXCR4 concentration in human MSCs are assessed by ELISA (CUSABIO, TX, USA).
166
167 *2.6 Immunohistochemistry for SDF-1 and CXCR4 expression*
168
169 Liver tissues and human MSCs are fixed in 10% neutral-buffered formalin, processed, and then

embedded in paraffin for light microscopy. Immunohistochemistry is performed following the standard avidin/streptavidin-biotin peroxidase methods. All slides (4 μM) are deparaffinized, rehydrated and boiled for antigen retrieval (30 m at 98°C in citrate buffer pH 6.0). Primary antibodies against SDF-1 (1:200) and CXCR4 (1:400) proteins (Abcam, USA) are used on the sections of the tumor tissue, with 1% BSA-PBS as the negative control. After being incubated overnight at 4°C, the slides are incubated with biotinylated anti-rabbit immunoglobulin for 30 min and then with horseradish peroxidase-jugated streptavidin for 30 min. Each step is followed by a washing with PBS. Staining is revealed by 3,3′-diaminobenzidine and counterstained with hematoxylin.

2.7 Model formulation

The population-level mathematical model includes the descriptions of MSC and SDF-1 kinetics in the blood and liver. After intravenous injection, MSCs are arrested in the liver from blood by both passive homing (via blood flow) and active homing (via the liver SDF-1 attracting CXCR4 in MSCs) (Karp et al., 2009). The number of MSCs in the liver can decrease due to a series of mechanisms including release back to the blood circulation and depletion. Here we refer to depletion as the loss of cell functionality and viability caused by various mechanisms (Oh et al., 2014; Wang et al., 2016). Therefore, the governing differential equation describing MSCs in the liver is as follows:

$$\frac{\mathrm{d}M_{\mathrm{L}}(t)}{\mathrm{d}t} = \overbrace{\alpha M_{\mathrm{B}}(t)}^{\text{Passive homing (via blood flow)}} + \overbrace{\beta S_{\mathrm{L}}(t)\left(1-\frac{M_{\mathrm{L}}(t)}{K}\right)}^{\text{Active homing (via SDF}-1/\text{CXCR4)}} - \overbrace{\gamma M_{\mathrm{L}}(t)}^{\text{Loss due to release and depleti}} \quad (1)$$

where $M_{\mathrm{L}}(t)$ (cell/kg) is the dose of MSCs in the liver, $M_{\mathrm{B}}(t)$ (cell/kg) is the dose of MSCs in the

191 blood, $S_L(t)$ (pg/mL) is the concentration of SDF-1 in the liver, t (h) is time, α (h^{-1}) is the MSC
192 arrest rate associated with blood flow, β (cell·mL/(kg·h·pg)) is the MSC arrest rate associated with
193 SDF-1/CXCR4 attraction, K (cell/kg) is the attraction capacity of MSCs expressing CXCR4
194 attracted by SDF-1 in the liver, and γ (h^{-1}) is the MSC loss rate in the liver including release and
195 depletion.

196

197 For MSCs in the blood, a relatively fast dose-decrease at early time, known as the distribution
198 phase, is followed by a slower decrease at later time, known as the elimination phase. These
199 processes can be modelled using a biexponential decay model (Armitage et al., 2003):

$$M_B(t) = \overbrace{C_1 e^{-\lambda_1 t}}^{\text{Distribution phase}} + \overbrace{C_2 e^{-\lambda_2 t}}^{\text{Elimination phase}} \quad (2)$$

200 where C_1 (cell/kg) and C_2 (cell/kg) are the intercepts for the distribution and elimination phases of
201 MSCs, and λ_1 (h^{-1}) and λ_2 (h^{-1}) are the decay rates for the distribution and elimination phases of
202 MSCs, respectively.

203

204 In normal mice, the SDF-1 concentration in the blood remains approximately constant. For SDF-
205 1 in the blood with an injured liver, the initial concentration is the same as that of normal uninjured
206 mice and increases at early reperfusion followed by a relatively slower decrease at later time.
207 Therefore the SDF-1 in the blood with an injured organ is modelled using the function form
208 associated with modified-biexponential decay (Wilson et al., 2015):

$$S_B(t) = \overbrace{S_B(0)}^{\text{Initial SDF}-1\text{ concentration}} + \overbrace{a_B e^{-b_B t}\left(1 - e^{-c_B t}\right)}^{\text{Kinetics of SDF}-1} \quad (3)$$

209 where $S_B(0)$ (pg/mL) is the initial concentration of SDF-1 in the blood of mice with injured liver,

a_B (pg/mL) is the amplitude of SDF-1 concentration change, b_B (h^{-1}) is the SDF-1 decay rate, and c_B (h^{-1}) is the control factor of SDF-1 kinetics.

In normal mice, the SDF-1 concentration in the liver remains approximately constant. SDF-1 concentration in the injured liver has the same function form as in the blood:

$$S_L(t) = S_L(0) + a_L e^{-b_L t}\left(1 - e^{-c_L t}\right) \quad (4)$$

where $S_L(0)$, $a_L = a_B/\eta_1$, $b_L = b_B/\eta_2$, and $c_L = c_B/\eta_3$ are the corresponding parameters in the liver that has the same physiological meanings as described in the model for SDF-1 kinetics in the blood. To develop the model on the basis of clinically accessible variables, the parameters for the SDF-1 in the organ are presented in terms of their relations with the corresponding parameters in the blood by association coefficients η_1, η_2, and η_3.

2.8 Model calibration

The calibration of the model is performed using MATLAB's nonlinear curve-fitting function, *lsqcurvefit* (MathWorks, 2018). Both models for SDF-1 and MSCs in the blood are calibrated with experimental data. The association coefficients η_1, η_2, and η_3 are then determined by comparing the calibrated models for SDF-1 in the blood and liver, and are validated by predicting the SDF-1 concentration in the liver based on the calibrated model for the SDF-1 concentration in the blood using published independent external data (Wilson et al., 2016). Details of the validation of the association coefficients are shown in the Supplemental Information. The calibrated models for

SDF-1 in the liver and MSCs in the blood are then inputted into the model for MSCs in the liver, to estimate the parameters in normal and injured livers, respectively.

3. RESULTS

3.1 Experimental results

Previous studies show that SDF-1 expression increases in the liver with ischemia/reperfusion (I/R) injury (Lentsch et al, 1999; Wilson et al., 2015). Our immunohistochemistry for SDF-1 in the mouse liver with ischemia/reperfusion (I/R) injury shows a significantly higher SDF-1level in the I/R injured liver than that the (Fig. 2A and C). A potential explanation is that with the presence of MSCs, SDF-1 is upregulated in the injured organs to attract and bind to MSC secreted CXCR4 (Lentsch et al, 1999; Wilson et al., 2015). Therefore, the high SDF-1 level can be considered as a maker for the SDF-1 and CXCR4 binding, indicating the increased number of MSCs in the I/R injured liver. To elucidate the SDF-1/CXCR4 regulated *in vivo* homing of human MSCs, we use droplet digital PCR assays for human-specific Alu sequences to quantify the numbers MSCs in the blood and liver of normal and hepatic I/R injured mice (Fig. 2D and E). Indeed, comparing the ELISA results for the normal and I/R injured livers (Fig. 2E) illustrates a higher MSC dose in the I/R injured liver.

In conjunction with Fig. 2A, Fig. 2B shows the overexpression of CXCR4 in hypoxia-preconditioned MSCs, which is consistent with previous experimental observations (Cencioni et al., 2012; Liu et al., 2012). Comparing with the normal MSCs, the CXCR4 expression in 24h hypoxia-preconditioned MSCs is about 4-fold higher. Previous studies find that the hypoxia

preconditioned MSCs also become more active in terms of both cell motility and proliferation (Ali et al., 2016; Beegle et al., 2015; Liu et al., 2012). Aligning with these experimental findings, our ELISA results show an increased number of hypoxia-preconditioned MSCs in the I/R injured liver comparing to the normal MSCs in the same liver condition. However, at this stage how the hypoxia-preconditioning facilitates *in vivo* homing of MSCs remains unclear. For example, it is unclear whether the hypoxic preconditioning enhances MSC homing through: (i) the SDF-1/CXCR4 chemotaxis (active homing); or (ii) the transportation via blood flow (passive homing); or (iii) a combination of effects from (i) and (ii)? We now attempt to distinguish between these two possibilities by calibrating our mathematical model to the experimental data.

3.2 Modelling results

The mathematical model for *in vivo* human bone marrow-derived MSC homing is developed based on the published intravital imaging details of administered MSCs (Toma et al., 2009; Wang et al., 2016) and SDF-1/CXCR4 chemotaxis of MSCs (Fig. 1A) (Dar et al., 2005; Ji et al., 2004). Following intravenous injection, MSCs are arrested in organs by both passive homing (via blood flow) and active homing (via the organ SDF-1 attracting CXCR4 expressing MSCs) (Karp & Teo, 2009). MSC release and depletion in organs are described by a single loss term in our model. Differentiation is not included in the model as differentiation is slow relative to the time scale of the experiment and hence would have a small impact on the MSC distribution at the organ level over the observation period (Hass et al., 2011; Schmidt et al., 2006). As shown in Fig. 1B, this model has two compartments: blood and injured organ (liver). All MSCs are assumed to act independently with no obligatory connections or intercellular feedback loops. In

summary, we assume the *in vivo* kinetics of MSCs are governed by two processes: (i) transport to the organ (liver) via blood flow and the SDF-1/CXCR4 chemotaxis; and (ii) loss in the organ by release and depletion. Variables included in the model are time t (h), SDF-1 concentration in blood $S_B(t)$ (pg/mL) and liver $S_L(t)$ (pg/mL), and MSC dose in blood $M_B(t)$ (cell/kg) and liver $M_L(t)$ (cell/kg).

Previous modelling of the *in vivo* homing of MSCs in organs neglects SDF-1/CXCR4 chemotaxis (Wang et al., 2016), while the biological evidence suggests that this mechanism plays an important role in the MSC homing (Abbott et al., 2004; Hu et al., 2013; Lentsch et al, 1999; Wilson et al., 2015). With the SDF-1/CXCR4 chemotaxis incorporated in our model, we calibrate the model system (Equations (1) - (4)) to the experimental data, as shown in Fig. 2C-E. The model captures key features of the observed time evolution of MSC dose in the mouse liver with a high goodness-of-fit, with R^2=0.987 (Supporting Information Fig. S1). The SDF-1 profiles in Fig 2C show that the SDF-1levels in the liver and blood are maximally increased after approximately 12 h of reperfusion, which correlates with maximal liver injury after hepatic I/R injury reported in previous studies (Lentsch et al, 1999; Wilson et al., 2015). Following intravenous injection, the MSC dose in the liver increases until 4 hours after injection, and then slowly declined. The area under the curve ($AUC_{0\text{-}48hr}$) of MSCs in the liver indicates that organ loading of MSCs (Fig. 2E) increases by 1.52 times following hepatic I/R injury (from 2.00×10^9 cells · h/kg to 3.05×10^9 cells · h/kg), and the organ loading of hypoxia-preconditioned MSCs (Fig. 2F) increases by 1.71 times (3.43×10^8 cells · h/kg). The increased organ loading suggests that the injured liver is an effective attractant for both normal and hypoxia-preconditioned MSCs.

The parameter estimates obtained by calibrating the model to match the experimental data are listed in Table 1. These parameter estimates reveal three important features:

1. Estimates of α, which represents the MSC arrest rate associated with blood flow, are approximately the same for all liver and MSC conditions. The small change (about 10%) in α estimates suggests that neither the liver nor MSC conditions have significant impact on the passive homing,

2. The highest SDF-1/CXCR4 attraction capacity and MSC arrest rate associated with SDF-1/CXCR4 attraction are obtained for the hypoxia-preconditioned MSCs in I/R injured livers. Both the SDF-1/CXCR4 attraction capacity and the corresponding MSC arrest rate significantly increase (over 100%) compared to those obtained for the normal MSCs in normal livers, indicating that SDF-1 in organs is an effective *in vivo* attractant for MSCs expressing CXCR4,

3. The MSC depletion rate is lower for the hypoxia-preconditioned MSCs than for the untreated MSCs, which is consistent with results from previous studies that hypoxic preconditioning enhances the MSC survival *in vivo* (Beegle et al., 2015; Liu et al., 2012). Based on our modelling results, we suggest that the hypoxic preconditioning enhances *in vivo* homing of MSCs though active homing and the survival of MSCs in the organ, whereas its impact on passive homing is small.

To further validate the model, simulations of SDF-1 levels in mouse blood and livers are compared with published data (Wilson et al., 2015). All parameters are obtained using the same approach described in the Methods section. As shown in Supplemental Information (Fig. S2), there is a high goodness-of-fit with R^2=0.986, between model predictions and the independent data, indicating that the model is suitable to characterize the *in vivo* kinetics of SDF-1. Our

model is then used to predict the *in vivo* homing of the MSCs administered at a different initial dose (1.5×10^6 cells/animal). All parameters in the model are maintained the same as shown in Table 1, and we find that the model adequately predicts the MSC doses in both normal and injured livers, again with a high goodness-of-fit with R^2 close to unity (Fig. 3). The good agreement between the model predictions and experimental data confirms that this model can be readily applied to different MSC dose regimens. There is substantial evidence that administered MSCs would accumulate within sites of disease or injury (Hu et al., 2013; Ji et al., 2004; Kitaori et al., 2009; Liu et al., 2012). However, previously published cytokinetic models often underestimate the therapeutic cell concentration in diseased organs such as the heart with myocardial infarction or fibrotic liver (Wang et al., 2016; Zhu et al., 1996). As our model includes the important SDF-1/CXCR4 axis which regulates the *in vivo* homing of stem cells to sites of injury, it is able to account for the effect of tissue injury on MSC distribution.

4. DISCUSSION

There is a growing interest in MSCs in the context of regenerative medicine for treating injured organs (Jiang et al., 2018; Squillaro et al., 2016; Zhang et al., 2017). Therefore, understanding the kinetics, including the homing of MSCs, is becoming crucial to improve treatment outcomes. Previous studies find that the SDF-1/CXCR4 axis is important in the homing of MSCs to injured organs, and help mobilization of the MSCs to injured tissues (Hu et al., 2013; Ji et al., 2004; Kitaori et al., 2009; Liu et al., 2012; Wilson et al., 2015). However, to the best of our knowledge, there are no mathematical models that capture features of the SDF-1/CXCR4 chemotaxis in injured organs at present. In this study we develop a mathematical model to characterize *in vivo*

345 homing of administered human bone marrow-derived MSCs. The model considers both MSC
346 and SDF-1 kinetics in the blood and organ and assumes that MSCs arrest in organs via both
347 passive homing through blood flow, and active homing through the organ SDF-1 attracting
348 CXCR4 in MSCs.
349
350 Our calibrated mathematical model captures the key features of the experimental data sets.
351 Comparing the parameter estimates for different cases illustrates that the liver and MSC
352 conditions have small impact on the passive homing mechanism. On the other hand, the hypoxia-
353 preconditioned MSCs result in a higher arrest rate associate with the SDF-1/CXCR4 chemotaxis
354 and a lower loss rate, and therefore lead to a higher MSC dose in the liver. As the hypoxia-
355 preconditioned MSCs are characterized by the overexpressed CXCR4, our modelling results
356 reveal the significance of the SDF-1/CXCR4 axis. The calibrated model also well predicts the
357 MSC dose initiated with a different amount. The model developed in this work is the first one
358 that describes and quantifies *in vivo* homing of MSCs via both passive and active mechanisms.
359 Although there is a lack of similar measured or estimated parameters in the literature to compare
360 with, the model provides insights into the impacts of SDF-1/CXCR4 axis on *in vivo* MSC
361 homing through the comparison of the parameter estimates for different liver and MSC
362 conditions. Since previous studies show that MSCs undergo similar processes arresting into
363 various organs (Abbott et al., 2004; Ji et al., 2004; Kucia et al., 2004; Liu et al., 2012; Squillaro
364 et al., 2016), our model can possibly be generalized to predict the MSC homing in other organs
365 by calibrating the model to other experimental datasets.
366
367 In most clinical settings, it is impossible to characterize the number of unlabeled MSCs in

organs. Since our model is developed on the basis of clinically accessible variables, such as MSC dose and SDF-1 concentration in blood, it may be further developed to predict the homing of MSCs in human bodies. This model can be more useful for clinical applications because it has a less complicated framework and fewer parameters than the previous ones; and enables a more efficient and rational design of MSC therapies by precise prediction of MSC homing to target organs with injury.

5. CONCLUSION

In summary, through the development of the model that incorporates the critical SDF-1/CXCR4 chemotaxis, we demonstrate that it is possible to predict the *in vivo* distribution of administered MSCs in normal and injured livers using clinically accessible variables. Our study provides proof-of-concept for the novel use of mathematical modelling to study the kinetics of MSCs in normal and injured organs for more efficiently designing stem cell-based therapies.

References

Abbott JD, Huang Y, Liu D, Hickey R, Krause DS, Giordano FJ. 2004. Stromal cell–derived factor-1α plays a critical role in stem cell recruitment to the heart after myocardial infarction but is not sufficient to induce homing in the absence of injury. *Circulation*. 110:3300-3305.

Ali NM, Boo L, Yeap SK, Ky H, Satharasinghe DA, Liew WC, Ong HK, Cheong SK, Kamarul T. 2016. Probable impact of age and hypoxia on proliferation and microRNA expression profile of bone marrow-derived human mesenchymal stem cells. *PeerJ*. 4: e1536.

Armitage WJ, Dick AD, Bourne WM. 2003. Predicting endothelial cell loss and long-term corneal graft survival. *Investigative Ophthalmology & Visual Science*. 44: 3326-3331.

Beegle J, Lakatos K, Kalomoiris S, Stewart H, Isseroff RR, Nolta JA, Fierro FA. 2015. Hypoxic preconditioning of mesenchymal stromal cells induces metabolic changes, enhances survival, and promotes cell retention *in vivo*. *Stem Cells*. 33:1818-1828.

Cencioni C, Capogrossi MC, Napolitano M. 2012. The SDF-1/CXCR4 axis in stem cell preconditioning. *Cardiovascular Research*. 94:400-407.

Chung HM, Cartwright MM, Bortz DM, Jackson TL, Younger JG. 2008. Dynamical system analysis of Staphylococcus epidermidis bloodstream infection. *Shock*. 30: 518-526.

Dar A, Goichberg P, Shinder V, Kalinkovich A, Kollet O, Netzer N, Margalit R, Zsak M, Nagler A, Hardan I, Resnick I. 2005. Chemokine receptor CXCR4–dependent internalization and resecretion of functional chemokine SDF-1 by bone marrow endothelial and stromal cells. *Nature Immunology*. 6:1038-1046.

Enderling H, Anderson AR, Chaplain MA, Beheshti A, Hlatky L, Hahnfeldt P. 2009. Paradoxical dependencies of tumor dormancy and progression on basic cell kinetics. *Cancer Research*. 69: 8814-8821.

Fu X, Jiang B, Zheng B, Yan Y, Wang J, Duan Y, Li S, Yan L, Wang H, Chen B, Sang X. 2018. Heterogenic transplantation of bone marrow-derived rhesus macaque mesenchymal stem cells ameliorates liver fibrosis induced by carbon tetrachloride in mouse. *PeerJ*. 6: e4336.

Futrega K, Palmer JS, Kinney M, Lott WB, Ungrin MD, Zandstra PW, Doran MR. 2015. The microwell-mesh: A novel device and protocol for the high throughput manufacturing of cartilage microtissues. *Biomaterials*. 62: 1-12.

Hass R, Kasper C, Böhm S, Jacobs R. 2011. Different populations and sources of human mesenchymal stem cells (MSC): A comparison of adult and neonatal tissue-derived MSC. *Cell Communication and Signaling*. 9:12.

Hu C, Yong X, Li C, Lü M, Liu D, Chen L, Hu J, Teng M, Zhang D, Fan Y, Liang G. 2013. CXCL12/CXCR4 axis promotes mesenchymal stem cell mobilization to burn wounds and contributes to wound repair. *Journal of Surgical Research*. 183:427-434.

Holzhütter HG, Drasdo D, Preusser T, Lippert J, Henney AM. 2012. The virtual liver: a multidisciplinary, multilevel challenge for systems biology. *Wiley Interdisciplinary Reviews: Systems Biology and Medicine*. 4: 221-235.

Ji JF, He BP, Dheen ST, Tay SS. 2004. Interactions of chemokines and chemokine receptors mediate the migration of mesenchymal stem cells to the impaired site in the brain after hypoglossal nerve injury. *Stem Cells*. 22:415-427.

Jin W, Penington CJ, McCue SW, Simpson MJ. 2016. Stochastic simulation tools and continuum models for describing two-dimensional collective cell spreading with universal growth functions. *Physical Biology*. 13:056003.

Jin W, Penington CJ, McCue SW, Simpson MJ. 2017. A computational modelling framework to quantify the effects of passaging cell lines. *PLOS ONE*. 12: e0181941.

Jin W, McCue SW, Simpson MJ. 2018. Extended logistic growth model for heterogeneous populations. *Journal of Theoretical Biology*. 445: 51-61.

Karp JM, Teo GSL. 2009. Mesenchymal stem cell homing: The devil is in the details. *Cell Stem Cell*. 4:206-216.

Kitaori T, Ito H, Schwarz EM, Tsutsumi R, Yoshitomi H, Oishi S, Nakano M, Fujii N, Nagasawa T, Nakamura T. 2009. Stromal cell-derived factor 1/CXCR4 signaling is critical for the recruitment of mesenchymal stem cells to the fracture site during skeletal repair in a mouse model. *Arthritis & Rheumatology*. 60:813-823.

Kucia M, Ratajczak J, Reca R, Janowska-Wieczorek A, Ratajczak MZ. 2004. Tissue-specific muscle, neural and liver stem/progenitor cells reside in the bone marrow, respond to an SDF-1 gradient and are mobilized into peripheral blood during stress and tissue injury. *Blood Cells, Molecules, and Diseases*. 32:52-57.

Lentsch AB, Yoshidome H, Kato A, Warner RL, Cheadle WG, Ward PA, Edwards MJ. 1999. Requirement for interleukin-12 in the pathogenesis of warm hepatic ischemia/reperfusion injury in mice. *Hepatology*. 30:1448-1453.

Liu H, Liu S, Li Y, Wang X, Xue W, Ge G, Luo X. 2012. The role of SDF-1-CXCR4/CXCR7 axis in the

therapeutic effects of hypoxia-preconditioned mesenchymal stem cells for renal ischemia/reperfusion injury. *PloS ONE*. 7:e34608.

Markway BD, Tan GK, Brooke G, Hudson JE, Cooper-White JJ, Doran MR. 2010. Enhanced chondrogenic differentiation of human bone marrow-derived mesenchymal stem cells in low oxygen environment micropellet cultures. *Cell Transplantation*. 19: 29-42.

MathWorks. 2018. lsqcurvefit. [ONLINE] Available at: http://au.mathworks.com/help/optim/ug/lsqcurvefit.html.

Niclis JC, Gantner CW, Hunt CP, Kauhausen JA, Durnall JC, Haynes JM, Pouton CW, Parish CL, Thompson LH. 2017. A PITX3-EGFP reporter line reveals connectivity of dopamine and non-dopamine neuronal subtypes in grafts generated from human embryonic stem cells. *Stem Cell Reports*. 9: 868-882.

Oh J, Lee YD, Wagers AJ. 2014. Stem cell aging: mechanisms, regulators and therapeutic opportunities. *Nature Medicine*. 20: 870-880.

Parekkadan B, Milwid JM. 2010. Mesenchymal stem cells as therapeutics. *Annual Review of Biomedical Engineering*. 12: 87-117.

Rohart F, Mason EA, Matigian N, Mosbergen R, Korn O, Chen T, Butcher S, Patel J, Atkinson K, Khosrotehrani K, Fisk NM. 2016. A molecular classification of human mesenchymal stromal cells. *PeerJ*. 4: e1845.

Schmidt A, Ladage D, Steingen C, Brixius K, Schinköthe T, Klinz FJ, Schwinger RH, Mehlhorn U, Bloch W. 2006. Mesenchymal stem cells transmigrate over the endothelial barrier. *European Journal of Cell Biology*. 85: 1179-1188.

Shim G, Lee S, Han J, Kim G, Jin H, Miao W, Yi TG, Cho YK, Song SU, Oh YK. 2015. Pharmacokinetics and *in vivo* fate of intra-articularly transplanted human bone marrow-derived clonal mesenchymal stem cells. *Stem Cells and Development*. 24: 1124-1132.

Squillaro T, Peluso G, Galderisi U. 2016. Clinical Trials With Mesenchymal Stem Cells: An Update. *Cell Transplantation*. 25: 829-848.

Toma C, Wagner WR, Bowry S, Schwartz A, Villanueva F. 2009. Fate of culture-expanded mesenchymal stem cells in the microvasculature: *In vivo* observations of cell kinetics. *Circulation Research*. 104: 398-402.

Wang H, Liang X, Xu ZP, Crawford DH, Liu X, Roberts MS. 2016. A physiologically based kinetic model for elucidating the in vivo distribution of administered mesenchymal stem cells. *Scientific Reports*. 6: 22293.

Werner B, Beier F, Hummel S, Balabanov S, Lassay L, Orlikowsky T, Dingli D, Brümmendorf TH, Traulsen A. 2015. Reconstructing the *in vivo* dynamics of hematopoietic stem cells from telomere length distributions. *eLife*. 4: e08687.

Werner B, Scott JG, Sottoriva A, Anderson AR, Traulsen A, Altrock PM. 2016. The cancer stem cell fraction in hierarchically organized tumors can be estimated using mathematical modeling and patient-specific treatment trajectories. *Cancer Research*. 76: 1705-1713.

Wilson GC, Freeman CM, Kuethe JW, Quillin 3rd RC, Nojima H, Schuster R, Blanchard J, Edwards MJ, Caldwell CC, Lentsch AB. 2015. CXC chemokine receptor-4 signaling limits hepatocyte proliferation after hepatic ischemia-reperfusion in mice. *American Journal of Physiology-Gastrointestinal and Liver Physiology*. 308: G702-709.

Wodarz D, Garg N, Komarova NL, Benjamini O, Keating MJ, Wierda WG, Kantarjian H, James D, O'Brien S, Burger JA. 2014. Kinetics of chronic lymphocytic leukemia (CLL) cells in tissues and blood during therapy with the BTK inhibitor ibrutinib. *Blood*. Blood-2014-02-554220.

Zhang F, Ren H, Shao X, Zhuang C, Chen Y, Qi N. 2017. Preservation media, durations and cell concentrations of

512 short-term storage affect key features of human adipose-derived mesenchymal stem cells for therapeutic application.
513 *PeerJ*. 5: e3301.
514
515 Zhao P, Zhang L, Grillo JA, Liu Q, Bullock JM, Moon YJ, Song P, Brar SS, Madabushi R, Wu TC, Booth BP.
516 2011. Applications of physiologically based pharmacokinetic (PBPK) modeling and simulation during regulatory
517 review. *Clinical Pharmacology & Therapeutics*. 89: 259-267.
518
519 Zhu H, Melder RJ, Baxter LT, Jain RK. 1996. Physiologically based kinetic model of effector cell biodistribution in
520 mammals: implications for adoptive immunotherapy. *Cancer Research*. 56: 3771-3781.

521
522

Figure 1

Hypothesis and schematic diagram of modeling *in vivo* homing of therapeutic MSCs.

(A) Schematic diagram of the stromal cell-derived factor-1 (SDF-1)/CXC chemokine receptor 4 (CXCR4) axis in *in vivo* homing of MSCs to the sites of hepatic ischemia/reperfusion (I/R) injury. The SDF-1 is upregulated at the sites of injury and serves as a potent chemoattractant to recruit circulating or residing MSCs expressing its cognate receptor CXCR4 on the surface. **(B)** Schematic of compartment model for *in vivo* homing of therapeutic MSCs.

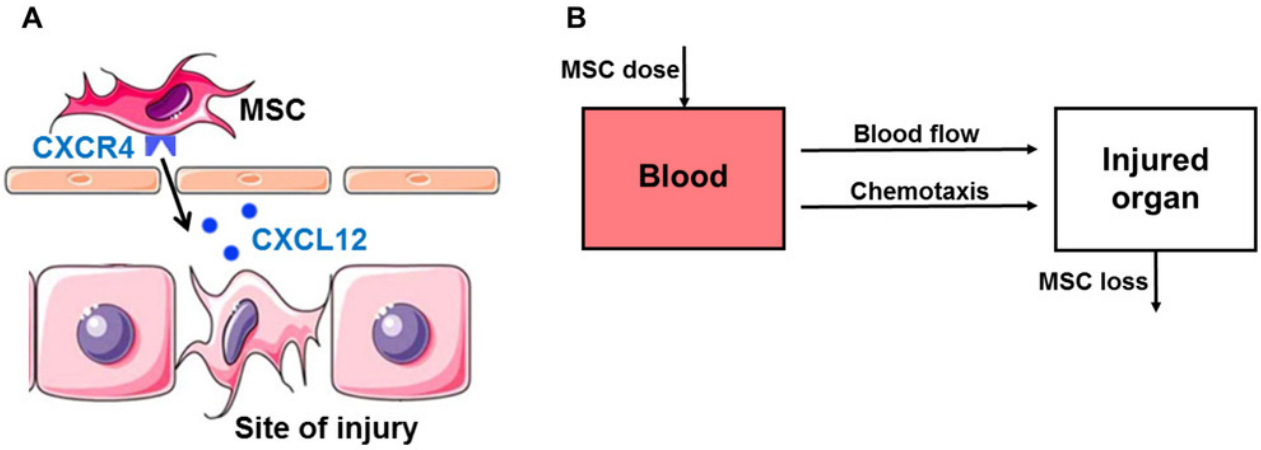

Figure 2

Model calibration results with experimental data.

(A) Representative micrographs of immunohistochemistry for CXCR4 in hypoxia-preconditioned MSCs (3% O_2) and SDF-1 in mouse liver with ischemia/reperfusion (I/R) injury. **(B)** CXCR4 levels in control MSCs and hypoxia-preconditioned MSCs (3% O_2). Quantitative ELISA was used for the analysis of CXCR4 levels in MSCs. **(C)** Model calibration with the SDF-1 concentrations in the blood and liver of mice with hepatic ischemia/reperfusion (I/R) injury. **(D)** Model calibration with the MSC doses in the blood of normal mice and mice with hepatic I/R injury at dose of 5×10^5 cells/animal. **(E)** Model calibration with the MSC doses in the liver of normal mice and mice with hepatic I/R injury at dose of 5×10^5 cells/animal. **(F)** Model calibration with the hypoxia-preconditioned MSC doses in the liver of mice with hepatic I/R injury at dose of 5×10^5 cells/animal. The solid line in each panel represents the concentration-time profile of the SDF-1 and MSCs simulated by the model while the circles represent measured data. The SDF-1 concentration and MSC dose are expressed as SDF-1 amount and number of cells per kilogram of tissue. The data are expressed as the sample mean ± sample standard deviation.

PeerJ Preprints | https://doi.org/10.7287/peerj.preprints.27144v1 | CC BY 4.0 Open Access | rec: 27 Aug 2018, publ: 27 Aug 2018

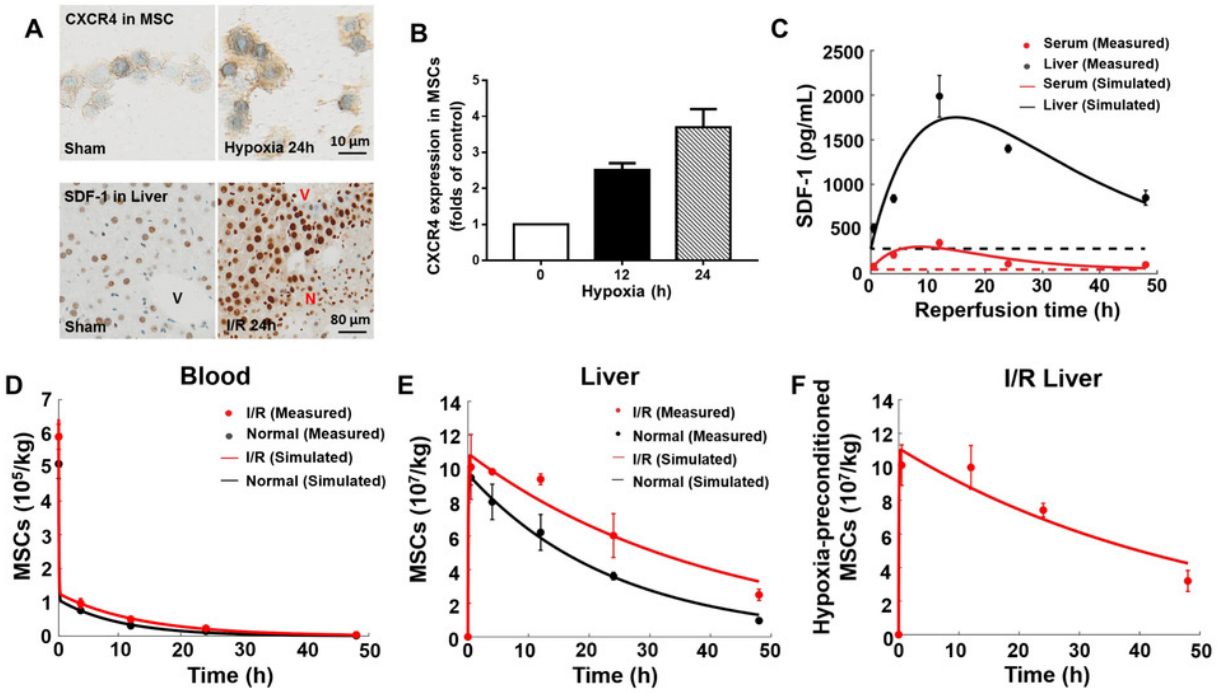

Figure 3

Model validation results with experimental data.

(A) Model validation with the MSC doses in the blood of normal mice and mice with hepatic I/R injury at an initial dose of 1.5 × 10^6 cells/animal. **(B)** Model validation with the MSC doses in the liver of normal mice and mice with hepatic I/R injury at a dose of 1.5 × 10^6 cells/animal. The solid line in each panel represents the concentration-time profile of the MSCs simulated by the model while the circles represent measured data. The MSC dose is expressed as the number of cells per kilogram of tissue. The data are expressed as the sample mean ± sample standard deviation. **(C)** Goodness-of-fit plot of model validation. Model predictions and experimental data were analyzed using linear regression, with R^2=0.969 (n = 16).

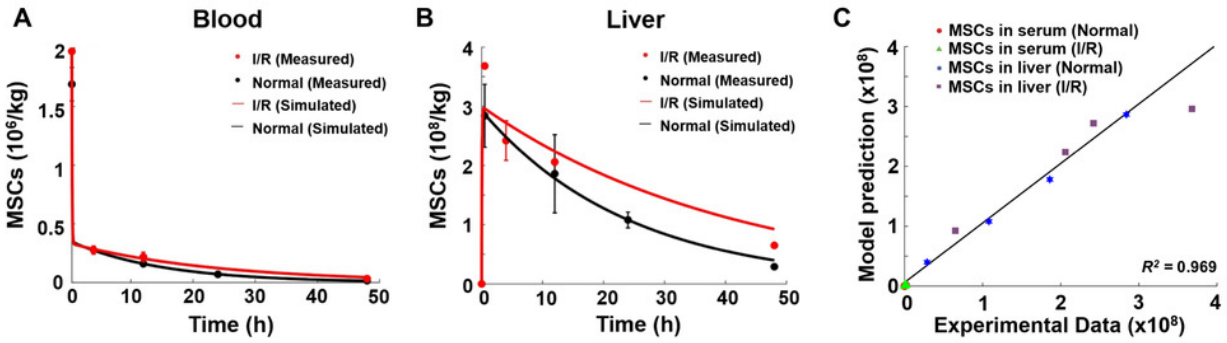

Table 1(on next page)

Values and reference of parameters in the model.

Table 1 Values and reference of parameters in the model

Parameter (unit)	Description	Dimensional			Reference
		Normal	I/R	I/R with hypoxia-preconditioning	
$S_B(0)$ (pg/mL)*	Initial SDF-1 in blood	48	-	-	Karp & Teo, 2009 and measured
a_B (pg/mL)**	Amplitude of SDF-1 concentration change	N/A	7.94×10^4	-	Estimated
b_B (h^{-1})	SDF-1 decay rate	N/A	0.11	-	Estimated
c_B (h^{-1})	Control factor of SDF-1 kinetics	N/A	0.001	-	Estimated
η_1	Association coefficient	N/A	0.30	-	Estimated
η_2	Association coefficient	N/A	1.73	-	Estimated
η_3	Association coefficient	N/A	1.00	-	Estimated
$S_L(0)$ (pg/mL)*	Initial SDF-1 in liver	278	-	-	Karp & Teo, 2009 and measured
C_1 (cell/kg)*	Intercept for the distribution phase of MSCs	2.94×10^9 (5×10^5 dose)	-	-	Estimated
		8.82×10^9 (1.5×10^6 dose)	-	N/A	
C_2 (cell/kg)**	Intercept for the elimination phase of MSCs	1.12×10^5 (5×10^5 dose)	1.31×10^5 (5×10^5 dose)	-	Estimated
		3.59×10^5 (1.5×10^6 dose)	3.38×10^5 (1.5×10^6 dose)	N/A	
λ_1 (h^{-1})*	Slope of the distribution phase of MSCs	17.52	-	-	Estimated
λ_2 (h^{-1})**	Slope for the elimination phase of MSCs	0.10 (5×10^5 dose)	0.08 (5×10^5 dose)	-	Estimated
		0.07 (1.5×10^6 dose)	0.04 (1.5×10^6 dose)	N/A	
α (h^{-1})*	MSC arrest rate associated with blood flow	0.64	0.71	0.72	Wang et al. 2016 and estimated
β (pg*h)	MSC arrest rate associated with SDF-1/CXCR4 attraction	0.01	0.12	0.19	Estimated
γ (h^{-1})	MSC loss rate in organ	0.04	0.03	0.02	Wang et al. 2016 and estimated
K (cell/kg)	SDF-1/CXCR4 attraction capacity in organ	4.63×10^6	5.29×10^6	2.20×10^7	Estimated

*: Same value for all organ and MSC conditions.
**: Same value for all MSC conditions.